Ceramics International 50 (2024) 35677–35687

Contents lists available at ScienceDirect

Ceramics International

journal homepage: www.elsevier.com/locate/ceramint

Combined TL and EPR study to elucidate the origin of luminescent emission from La-doped CaF_2 phosphor

Jessica Mosqueira-Yauri [a], T.K. Gundu Rao [a], Joel A. Rivera-García [a], Klinton V.T. Huahuasoncco [a], Jorge S. Ayala-Arenas [a], J.F. Benavente [b], L.M. Rondán-Flores [c], José F.D. Chubaci [d], Nilo F. Cano [a,e,*]

[a] Universidad Nacional de San Agustín de Arequipa - UNSA, Arequipa, Peru
[b] CIEMAT, Av. Complutense 40, E, 28040, Madrid, Spain
[c] Instituto Pesquisas Energéticas e Nucleares, IPEN-CNEN/SP, São Paulo, SP, Brazil
[d] Universidade de São Paulo, Instituto de Física, São Paulo, SP, Brazil
[e] Universidade Federal de São Paulo - UNIFESP, Instituto do Mar, Santos, SP, Brazil

ARTICLE INFO

Handling Editor: Dr P. Vincenzini

Keywords:
La-doped CaF_2 phosphor
Defect centers
Luminescence
TL
EPR

ABSTRACT

This paper presents the results of the combined study of the thermoluminescence (TL) and electron paramagnetic resonance (EPR) properties of La-doped CaF_2 (CaF_2: La) phosphor. X-ray diffraction (XRD) results confirmed that CaF_2 has been successfully synthesized. Scanning electron microscopy (SEM) results and energy dispersive spectrometer (EDS) spectra show that the synthesized phosphor is pure and has a good overall morphology. The glow curve of CaF_2: La phosphor shows an emission band between 230 and 500 nm centered at 340 nm. The Tm-Tstop method and the deconvolution technique were used to find the number of overlapping TL peaks in the 50–300 °C region and their kinetic parameters. A linear dose-response curve was obtained for the range 1–9 Gy, with the onset of a slight supralinear behavior for doses higher than 9 Gy. Gamma-irradiated CaF_2: La phosphor has been studied using the technique of EPR to identify the defect centers and also to infer the centers involved in the TL process. Thermal annealing studies indicate the presence of three defect centers. One of the centers (center I) is identified as the O_2^- ion and is characterized by an axial g-tensor with principal values $g_\parallel = 2.013$ and $g_\perp = 2.0053$. This center correlates with the TL peak at 200 °C. Center II with an isotropic g-value of 2.0005 is attributed to an F center and also relates to the 200 °C TL peak. The third center (center III) is assigned to an F center.

1. Introduction

Rare earth-doped CaF_2 phosphors have attracted great attention in all areas of science and technology due to their interesting physicochemical properties and their potential applications in many new areas of scientific interest. Among them, we can highlight radiation dosimetry by luminescence. In this context, dopants play an important role in obtaining materials with high radiation sensitivity. The sensitivity of the material is generally due to defect centers formed during the synthesis of the material.

Identifying the defect centers responsible for the luminescent emission is fundamental to understanding the transfer mechanisms during the luminescent emission process. In addition, it allows for the establishment of dopant quantities to improve their luminescent properties and thus establish the suitability of the material for a given application in dosimetry. In this sense, electron paramagnetic resonance spectroscopy (EPR) is a sensitive technique that allows for the detection of unpaired electrons in a material, allowing for the acquisition of information about the electronic structure of the defects or paramagnetic centers.

CaF_2 presents important optical properties and the high solubility of rare earth, making it possible to use the material in radiation dosimetry [1–3]. For this reason, many synthetic crystals have been investigated, considering different amounts of dopants and different synthesizing techniques for sensitizing the CaF_2 crystal. CaF_2 can be obtained by many techniques, the most common being combustion, precipitation, liquid phase, solid-state reaction, and sol-gel [4–8].

Salah et al. [9] obtained TL results of CaF_2 doped with Eu, Cu, Ag,

---

* Corresponding author. Universidade Federal de São Paulo - UNIFESP, Instituto do Mar, Santos, SP, Brazil.
E-mail addresses: nilocano@if.usp.br, nilo.cano@unifesp.br (N.F. Cano).

https://doi.org/10.1016/j.ceramint.2024.06.385
Received 14 April 2024; Received in revised form 19 June 2024; Accepted 27 June 2024

and Tb exposed to gamma rays. The TL curve shows weak glow peaks below 125 °C, whereas the Dy-doped one is found to be highly sensitive, with a prominent peak at 165 °C.

Vasconcelos et al. [10] studied CaF_2 doped with Tm synthesized by liquid phase technique and obtained a material very sensitive to radiation with a good thermoluminescence response for samples irradiated with ^{60}Co gamma radiation, showing a linear response up to 10 kGy.

Aşlar and Şahiner [11] investigated the thermoluminescent response of commercial CaF_2: Dy dosimeters on the effect of three different irradiation sources (^{90}Sr/^{90}Y, ^{137}Cs, and X-rays). The CaF_2: Dy dosimeters show a good response for all three irradiation sources, with similar glow curves for all sources. Also, they investigated the effect of daylight on the TL of this material, showing a decay of TL intensity as a function of light exposure time.

Rodriguez et al. [12] studied pellets obtained from the simple mixture of calcium fluoride (CaF_2) and thulium oxide (Tm_2O_3) to improve the TL response of CaF_2. According to the authors, during the preparation, trapping centers were created due to new intrinsic defects in the CaF_2 matrix resulting from the mixture with thulium oxide.

Xie et al. [13] prepared CaF_2 co-doped with Nd and La by the coprecipitation technique. Compared with CaF_2: Nd, Y ceramics, CaF_2: Nd, La ceramics have a longer luminescence lifetime due to the larger radius of La^{3+} ions at the same doping concentration.

Vasconcelos et al. [14] produced Tm-doped CaF_2 by the combustion method. These authors show that CaF_2 phosphor doped with 0.2 mol% of Tm and heat treatment at 400 °C for 8 h after synthesis presents the best TL response, with a stable glow peak at about 175 °C and an emission band between 455 and 482 nm.

Recently, Rivera-Garcia et al. [15] synthesized and investigated the TL properties of CaF_2 phosphor doped with different concentrations of Ce. By XRD analysis, they showed the formation of a well-defined crystal structure of CaF_2 without any interference of the Ce dopant in the structure. The sample doped with 0.3 mol% of Ce presented the best TL response for two glow peaks at 120 and 280 °C, with the latter being the most stable at room temperature. Based on correlation studies between TL results and EPR, the authors identified the defect centers responsible for the TL emission of this material.

As we can see, the CaF_2 crystal was synthesized using different techniques and doped with different rare earths to improve its luminescence properties. Despite the interesting luminescence properties of CaF_2 doped with La and Dy or La and Nd, the study of CaF_2 doped only with La has not yet been performed. Therefore, in this work, we synthesized the La-doped CaF_2 crystal by precipitation followed by the combustion technique to study its TL and EPR properties. In addition, we performed correlation studies between TL and EPR results to identify the point defect centers responsible for the luminescence of the material. Some investigations on the EPR properties of CaF_2 have been carried out to study the defect centers and their importance as color centers of the material [13,14]. However, there is no combined study between TL and EPR results to elucidate the defect centers responsible for TL emission for La-doped CaF_2.

2. Materials and methods

La-doped calcium fluoride phosphor (CaF_2: La) was synthesized using a modified combustion route. For which, a precipitated material was obtained from the mixture of calcium nitrate tetrahydrate (Ca $(NO_3)_2$–$4H_2O$), ammonium fluoride (NH_4F), lanthanum nitrate hexahydrate (La $(NO_3)_3$–$6H_2O$) as dopant, and urea ($CO(NH_2)_2$) as fuel, and then the combustion procedure was performed. All the chemicals used for the synthesis are of high purity and were purchased from Merck Company.

X-ray diffraction (XRD) measurements of the synthesized phosphors were carried out using a Rigaku MiniFlex model 600 diffractometer with CuKα radiation. The XRD measurements were taken at the interval of Bragg angle 2θ ($20^\circ \leq 2\theta \leq 80^\circ$) with 0.005° step size and speed 4°/min at room temperature, in all cases, measurements were taken in triplicate. Morphology analysis of the CaF_2: La phosphors was performed using a Jeol JSM-IT700HR scanning electron microscope coupled to a Jeol energy dispersive spectroscopy (EDS) microanalysis system.

TL glow curves were recorded using a Harshaw model 3500 TL reader with a linear heating rate of 4 °C/. On the other hand, TL emission spectrum measurements were recorded using a Risø TL/OSL reader (DA20) and a monochromator placed under the photomultiplier tube of the TL reader.

EPR spectra were measured using a Freiberg Instruments MiniScope MS5000 spectrometer at room temperature and operating at X-band frequency. All EPR measurements were performed using 150 mg of the powdered sample placed in a quartz tube with an internal diameter of 4 mm. The equipment parameters used are: sweep time: 120 s, modulation amplitude: 0.1 mT, modulation frequency: 100 kHz, microwave power of 0.1 and 20 mW.

For TL measurements, the samples were irradiated with doses between 1 and 11 Gy using a ^{60}Co gamma source with a dose rate of 97.3 mGy/min, and for TL emission spectrum measurements, the CaF_2 phosphor samples were irradiated with ^{90}Sr/^{90}Y beta irradiation with a dose rate of 0.069 Gy/s. For EPR measurements, CaF_2 phosphors were irradiated with a dose of 500 Gy, 2.5 kGy, and 10 kGy using a ^{60}Co source with a dose rate of 379.43 Gy/h.

3. Results and discussion

The crystal structure, crystallinity, and crystallite size of the synthesized samples for different La concentrations (x = 0.1, 0.2, 0.3, and 0.4 mol%) were characterized by XRD. The results indicate that the synthesized products exhibit high purity and good crystallinity (see Fig. 1(a)). The XRD patterns were compared with ICDD file no. 77–2245, and the recorded data agree well with the CaF_2 XRD database with centered cubic phase and Fm3m space group. For a more detailed analysis of possible alterations with dopant concentration, the position of the main peak (111) has been plotted as a function of lanthanum

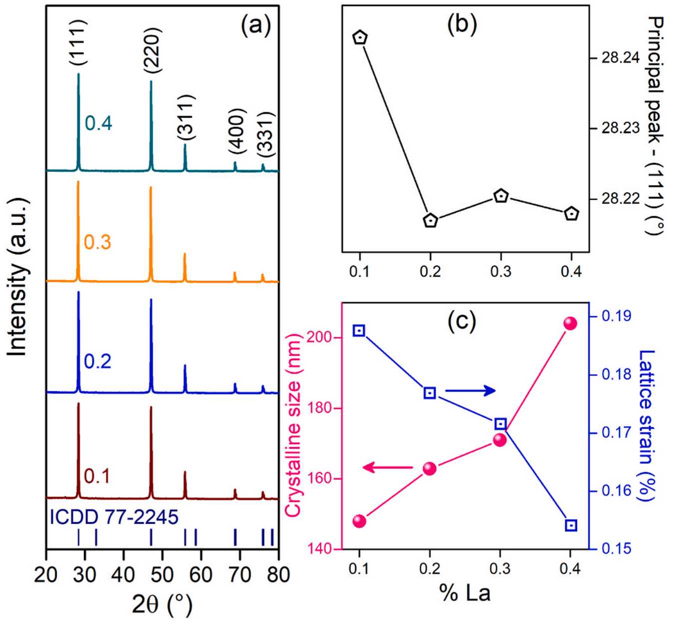

Fig. 1. (a) Typical XRD diffraction pattern plots of the CaF_2 phosphor for different concentrations of La. The dark blue vertical lines indicate the Bragg positions of the CaF_2 pattern. (b) Principal peak (111) of the CaF_2 phosphors as a function of La concentration. (c) Crystalline size and lattice strain in percentage of the CaF_2 phosphors as a function of La concentration. (For interpretation of the references to color in this figure legend, the reader is referred to the Web version of this article.)

dopant concentration. Fig. 1(b) shows a slight shift of the main peak toward a lower 2θ value between the 0.1 and 0.2 mol% concentrations. However, for the following concentrations, the position of the main peak remains at the same value, demonstrating that the material's crystal lattice structure is not affected by doping of 0.2, 0.3, and 0.4 mol% La.

The crystallite size (D_s) was evaluated by the Debye-Sherrer equation (equation (1)).

$$D_s = \frac{k\lambda}{B_{hkl}\cos\theta} \tag{1}$$

where λ is the X-ray wavelength (0.1541 nm), θ is the diffraction angle, κ is the shape factor ($\kappa = 0.9$), and B_{hkl} is the width (full-width at half-maximum) of the X-ray diffraction peak. $B_{hkl} = B_{obs} - B_{inst}$, where B_{obs} is the experimental peak broadening of a sample pattern, B_{inst} is the instrumental peak broadening computed from a standard pattern of Si. Table 1 shows the B_{hkl} of the main peak (111), crystallite size, and lattice strain induced due to crystal imperfections and distortions for the La-doped CaF_2 samples.

Fig. 1(c) shows the crystallite size behavior of phosphor CaF_2 as a function of dopant concentration. The particle size of the material increases with dopant concentration. On the other hand, the lattice strain of all samples decreases regularly with the dopant concentration; their values are less than 0.19 % throughout, confirming high crystallinity in each case.

To study the effect of the dopant concentration on the lattice parameters, we performed Rietveld refinement of the experimental XRD data using the X'Pert HighScore Plus program, with reference code ICDD 01-077-2245, which corresponds to calcium fluoride. Fig. 2 shows the Rietveld refinement for the sample doped with 0.3 mol% La using the Pseudo-Voigt function. The refinement data confirms the centered cubic phase structure and the Fm3m space group for all CaF_2 samples. Table 2 shows the refinement parameters, lattice parameters, and volume for the La-doped CaF_2 samples.

Fig. 3 shows the SEM image and energy dispersive spectrometer (EDS) spectrum of La-doped CaF_2 phosphor. Fig. 3(a and b) represents the homogeneous morphology of particle agglomerations with irregular geometry and different sizes that cluster together to form larger particles. A similar result was obtained by Gonzalez et al. [16] for Ce-doped CaF_2 phosphor. According to the particle size distribution histogram, the average particle size is 210 ± 95 nm, as shown in Fig. 3(c), which agrees well with the results obtained by XRD. On the other hand, the elemental mapping profiles (Fig. 3(d) to 3(f)) and EDS spectrum (Fig. 3(g)) of an agglomerate of CaF_2: La particles confirm the presence of calcium (53.17 wt %) and fluorine (46.36 wt %) uniformly distributed together with the lanthanum dopant. These results are in agreement with the stoichiometric calculations previously performed to synthesize the material. A similar result was obtained by Gonzales et al. [16] for Ce and Dy-doped CaF_2 phosphor synthesized by chemical reaction.

Fig. 4 shows the TL glow curves of CaF_2 phosphors doped with different La concentrations (x = 0.1, 0.2, 0.3, and 0.4 mol%). The TL glow curves were recorded after irradiation with gamma radiation at a dose of 1 Gy, using a linear heating rate of 4 °C/s in a temperature range of 50–300 °C. It is observed that the TL intensity is minimum for CaF_2 phosphors doped with 0.1 mol% La, and that of CaF_2 phosphors doped with 0.3 mol% is higher than that of CaF_2 phosphors doped with 0.2 and 0.4 mol%. Moreover, after increasing the La concentration above 0.4 mol%, the TL intensity decreases. The position of the first peak in the region from 110 to 120 °C remains invariant with the dopant concentration, except for the concentration of 0.1 mol%. On the other hand, the second peak shifts slightly with increasing La concentration. Therefore, the sample of CaF_2 phosphor doped with 0.3 mol% La has been selected for further analysis. The positions of the peaks of the 0.3 mol% doped phosphors are recorded at 115 and 205 °C.

Another result of TL emission is the efficiency of the phosphor glow curve response as a function of gamma irradiation dose. The glow curves of the CaF_2: La sample were measured by varying the gamma irradiation dose in the range from 1 to 11 Gy, and it was observed that the TL intensity increases with the gamma irradiation dose (Fig. 5(a)). Two slightly overlapping peaks centered at 130 and 205 °C appear in the TL glow curve. The existence of other possible overlapping peaks is further analyzed by Tm-Tstop and deconvolution methods. In principle, as the gamma irradiation dose increases, the trap density increases due to the formation of a large number of charge carriers that are trapped in centers or levels located within the forbidden band, and during the heating

Table 1
The full-width at half-maximum of the main peak (111), crystallite size, and deformation of CaF_2 phosphors doped with different concentrations of La.

La concentration (mol%)	B_{hkl} of the main peak (111) (°)	Crystallite size (nm)	Lattice strain (%)
0.10	0.05476	147.92	0.1876
0.20	0.04975	162.83	0.1769
0.30	0.04737	171.00	0.1716
0.40	0.03970	204.04	0.1541

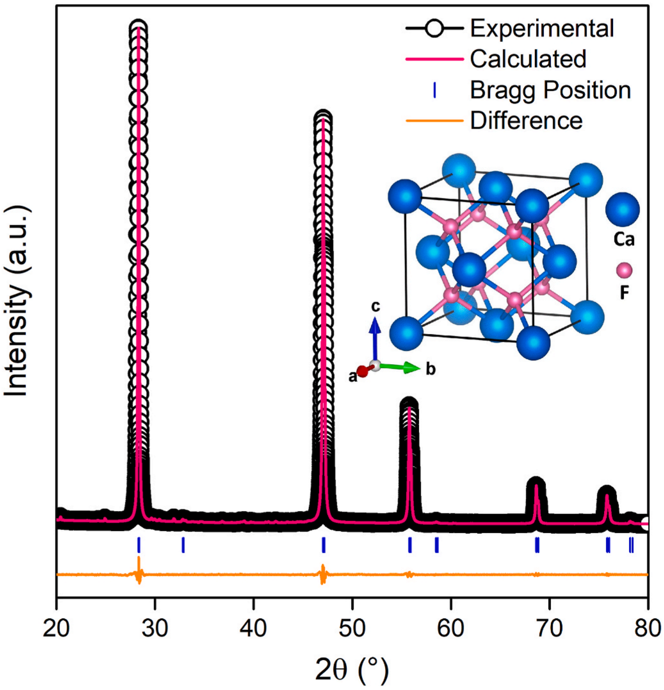

Fig. 2. Powder XRD pattern of the La-doped CaF_2 sample. Experimental (black circles), calculated (pink line), and residual (orange line) diffraction patterns. Bragg reflections of CaF_2 are indicated by blue vertical lines. The face-centered cubic crystal structure of the CaF_2 phosphor unit cell is shown in the inset of the figure. (For interpretation of the references to color in this figure legend, the reader is referred to the Web version of this article.)

Table 2
The Rietveld refinement parameters, lattice parameters, and volume of CaF_2 phosphors doped with different concentrations of La.

La concentration	Refinement parameters			Lattice parameters		Volume
(mol%)	R_p	R_{wp}	χ^2	a, b and c (Å)	α, β and γ (°)	(Å^3)
0.10	9.04	13.77	3.05	5.4623	90	192.98
0.20	8.94	13.05	3.13	5.4628	90	162.97
0.30	8.72	12.75	2.96	5.4641	90	163.14
0.40	8.51	12.80	3.01	5.4639	90	163.12

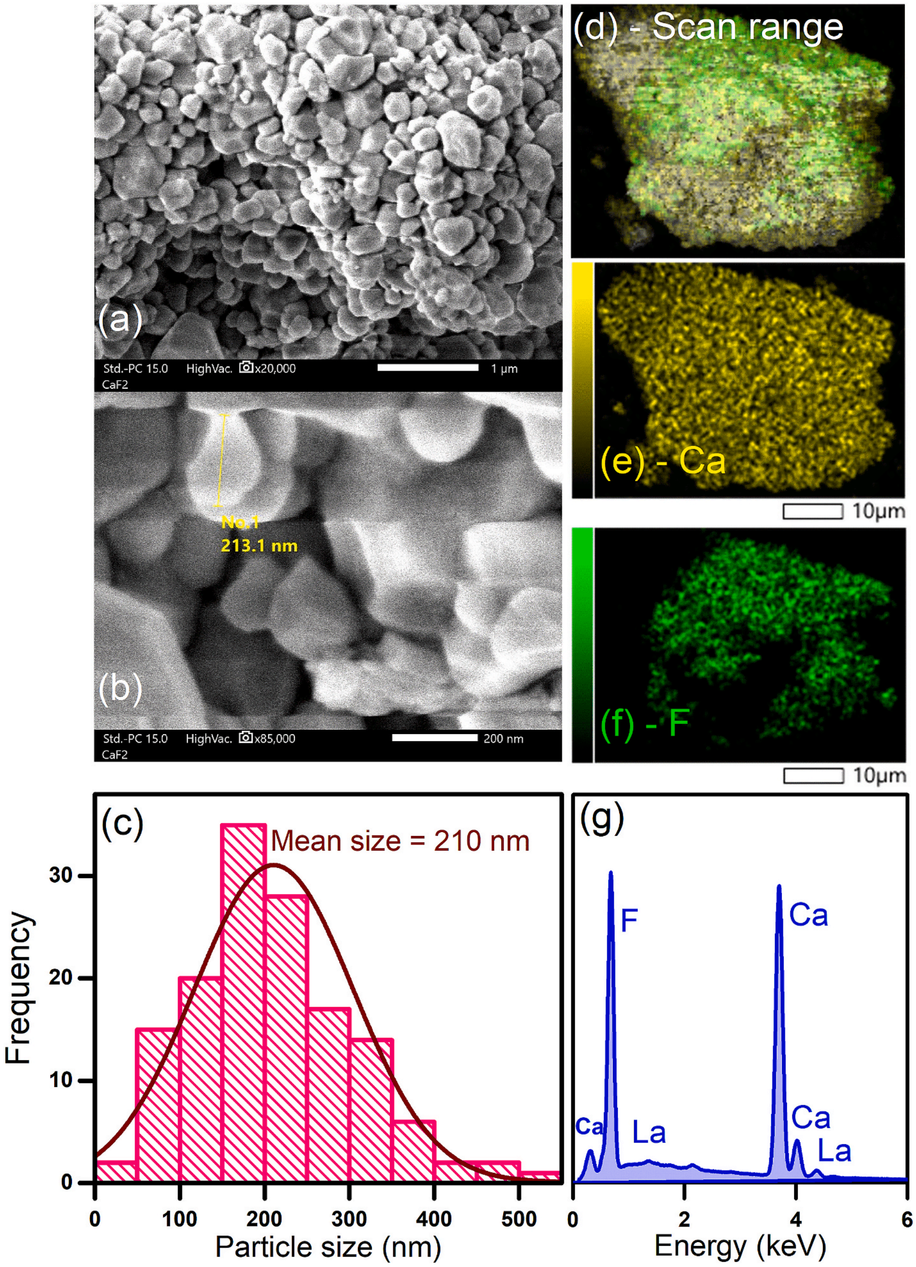

Fig. 3. (a) SEM image at a magnification of 20000. (b) SEM image at a magnification of 85000. (c) Histogram showing particle size distribution. (d–f) EDS analysis showing the distribution of Calcium and fluorine in CaF_2 phosphor. (g) Spectra showing the main components present in CaF_2, demonstrating that the presence of Ca and F.

or TL reading, depending on the dose applied, the charge carriers are released to recombine. The increase in the charge carrier density generates an increase in the TL intensity.

Since the TL intensity varies proportionally to the absorbed gamma dose, for possible dosimetric applications, it is very important to have a linear variation between the TL intensity and the absorbed dose. The linearity of the TL response of CaF_2: La phosphor was analyzed using the linearity index $f(D)$, defined by equation (2) [17].

$$f(D) = \frac{\frac{S(D)}{D}}{\frac{S(D_1)}{D_1}} \tag{2}$$

where $S(D)$ is the TL intensity for dose D, and D_1 is the lowest dose in the linear dose interval analyzed. When $f(D) = 1$ indicates the linearity interval, $f(D) > 1$ indicates supra-linearity, and $f(D) < 1$ indicates sublinearity. Fig. 5(b) at the top shows the TL intensity behavior as a function of dose for the peaks centered at 130 and 205 °C, and at the bottom shows the linearity index $f(D)$. Both peaks show linear behavior in the range from 1 to 9 Gy. For higher doses above 9 Gy, it shows a slight supra-linear growth.

The effect of temperature on TL emission is characterized by the shape of the glow curve, which is generally the superposition or sum of several individual peaks, which correspond to several electron traps associated with defect centers with a given energy depth (E). Therefore, the glow curve needs to be separated into its components, or peaks, to then find the kinetic parameters associated with each TL peak. To establish the number of peaks and their position, the Tm-Tstop and deconvolution methods have been used in combination.

Initially, we employ the Tm-Tstop method to obtain information about the positions of the constituent glow peaks of the glow curve [17]. The Tm-Tstop method helps to separate the overlapping peaks and

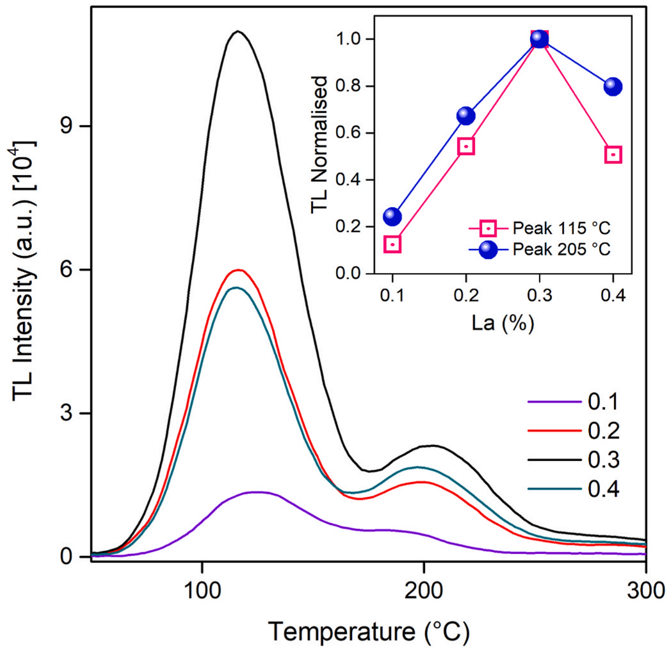

Fig. 4. TL glow curve for CaF_2 phosphor doped with 0.1, 0.2, 0.3, and 0.4 mol % of La. The inset shows the behavior of the maximum intensity of each peak as a function of La dopant concentration.

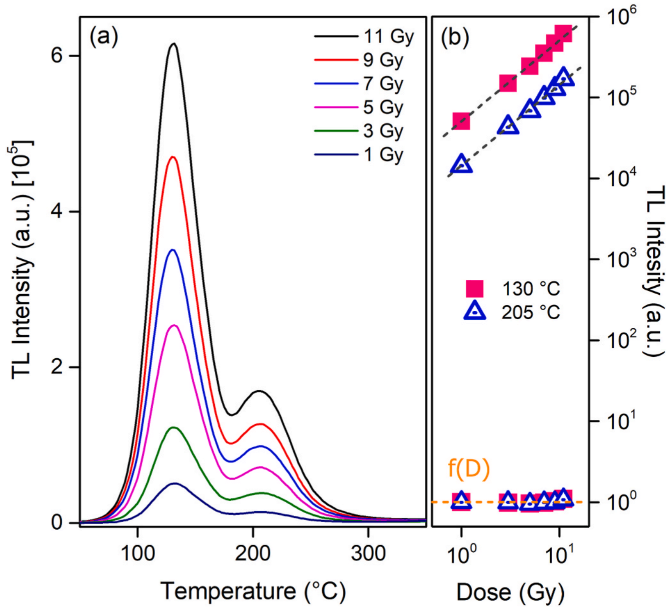

Fig. 5. (a) TL glow curve for CaF_2: La phosphor under gamma exposure for doses from 1 to 11 Gy. (b) TL intensity behavior as a function of gamma radiation dose (top) and the linearity index for peaks at 130 and 205 °C (bottom), the orange line represents the linearity index. (For interpretation of the references to color in this figure legend, the reader is referred to the Web version of this article.)

determine the approximate value of the peak temperature for each of them. Plateau regions on the Tm-Tstop plot indicate the presence of peaks with first-order kinetics (FOK), and sloping regions may indicate the presence of peaks with kinetics other than $b = 1$, or may also indicate peaks with first-order kinetics with continuous energy distribution.

For the Tm-Tstop analysis, 41 aliquots of CaF_2: La were irradiated with 5 Gy, and then we recorded the glow curve at different Tstop temperatures from 60 to 260 °C with 5 °C steps. The behavior of Tm as a function of Tstop is shown in Fig. 6. The plot shows the presence of six regions with different behaviors. This result indicates that the CaF_2: La glow curve presents at least six overlapping peaks in the temperature range from 60 to 260 °C. As the Tstop increases, it is only possible to observe a plateau, corresponding to the first region. For the other regions, an increase in Tm relative to Tstop is observed. However, this increase is not monotonic; jumps between regions are observed, and each region has a completely different increase from the others, indicating the presence of overlapping TL peaks. The invariance of the position of the peaks observed in Fig. 5 and the Tm-Tstop results show the presence of TL peaks that obey first-order kinetics (FOK), with the first peak corresponding to traps with localized energy distribution and the other five peaks corresponding to traps with continuous energy distribution.

On the other hand, the superposition of broad peaks can be solved using computational methods of glow curve deconvolution (CGCD) [18] using mathematical models based on band theory. Thus, using the preliminary analysis of the Tm-Tstop result that evidenced a complex trap structure with localized and/or continuous energy distributions, all glow curves were complemented by the CGCD method to obtain the number of peaks and their kinetic parameters for each peak. Fig. 7 illustrates the close similarity between the experimental and theoretical glow curve obtained by deconvolution by the CGCD method for samples irradiated between 1 and 11 Gy. A figure of merit (FOM) [19] less than 2.0 shows a good fit between the experimental and CGCD-calculated results. The position of the peaks, and the parameters of the traps for each dose are shown in Tables 3 and 4. In addition, the lifetime of the TL peaks at room temperature has been determined, and the results are presented in Tables 3 and 4 The lifetime values of the TL peaks and the linearity of the TL intensity as a function of radiation dose (see Fig. 5(b)) indicate that this material has potential application in clinical dosimetry, specifically in radiotherapy applications [20–22].

The mathematical model utilized to perform the deconvolution fitting of the experimental curves is based on a linear combination of six functions, as shown in the following expression:

$$I_{TL}(T) = {}^{1}\mathrm{F}^{\mathrm{FOK}}_{\mathrm{localized}}\left(E_1, {}^{1}T_{\mathrm{Max}}, {}^{1}I_{\mathrm{Max}}, b; T\right) + \sum_{i=2,3,4,5} {}^{\mathrm{i}}\mathrm{F}^{\mathrm{FOK}}_{\mathrm{continuous}}\left(E_{\mathrm{i}}, {}^{i}T_{\mathrm{Max}}, {}^{i}I_{\mathrm{Max}}, \sigma; T\right) \quad (3)$$

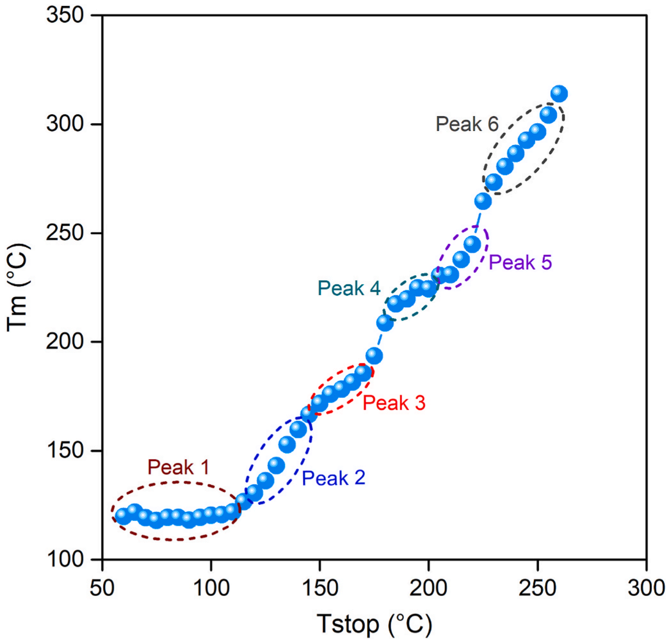

Fig. 6. Tm-Tstop plot for TL glow curve of CaF_2La phosphor. Dashed lines indicate the temperature region for the TL peaks of the glow curve.

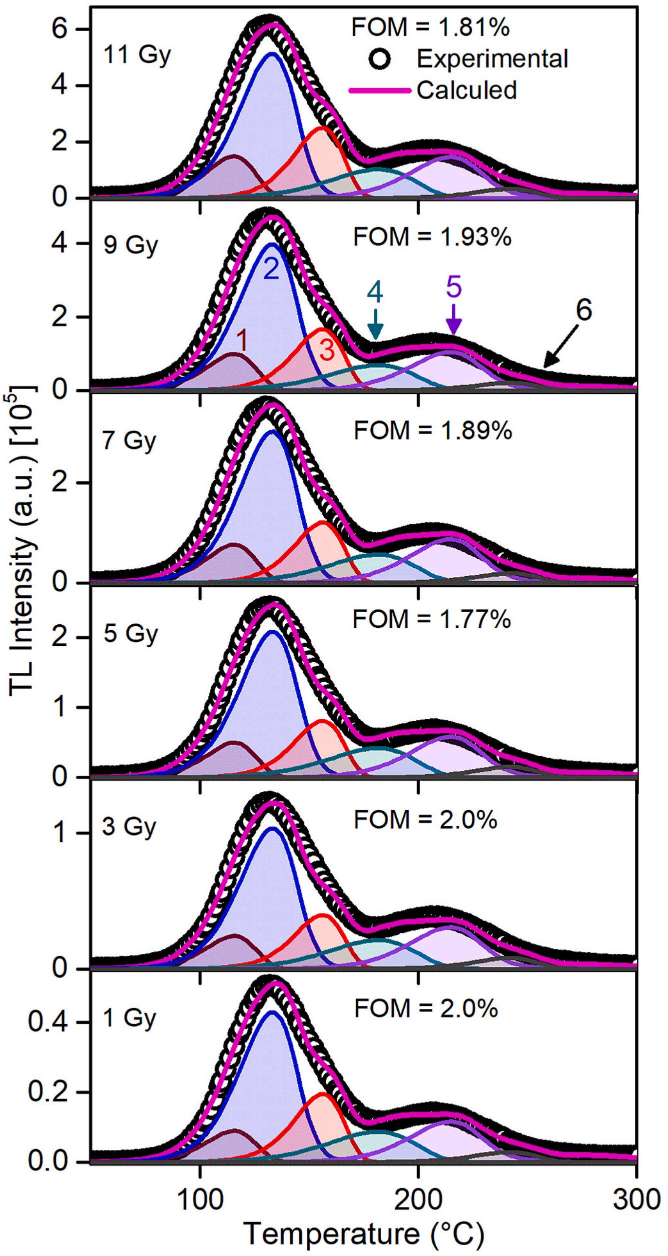

Fig. 7. Glow curve deconvolution graph for CaF_2: La phosphor irradiated with gamma doses of 1, 3, 5, 7, 9, and 11 Gy. First-order kinetics (FOK) with continuous energy distribution was used for all peaks, except for peak 1 with localized energy distribution.

If the FOK approach assumes, following equation is used:

$$^{FOK}I_n(T) = \frac{s}{\beta} \cdot \int_0^{+\infty} n(E) \cdot e^{-E/KT} \cdot exp\left(-\frac{s}{\beta} \int_{T_0}^{T} e^{-E/KT} \cdot dT \right) \cdot dE \qquad (4)$$

where $n(E)$ corresponds to the density of the trapped charge function, for continuous trap distributions related to exponential ones, the expression can be written:

$$n_{Gauss}(E) = n_0 \bullet f(E) = \frac{n_0}{\sqrt{2\pi\sigma^2}} \cdot e^{-(E_0 - E)^2 / 2 \cdot \sigma^2} \qquad (5)$$

and for localized distributions:

$$n_{Local}(E) = n_0 \bullet f(E) = n_0 \bullet \delta(E - E_0) \qquad (6)$$

Table 3
Details of activation energy (E), maximum temperature (T), distribution width (σ), frequency factors (s), and lifetime (τ) of the TL traps of the peaks 1, 2, and 3 of the CaF_2:La phosphor obtained by the deconvolution method of the glow curves for different doses. Bottom: the average.

Dose (Gy)	FOM (%)	Peak 1: FOK (Localized)				Peak 2: FOK (Continuous)					Peak 3: FOK (Continuous)				
		E (eV)	T (°C)	s (s^{-1})	τ (year)	E (eV)	σ (eV)	T (°C)	s (s^{-1})	τ (year)	E (eV)	σ (eV)	T (°C)	s (s^{-1})	τ (year)
1	2.00	1.1314	115.58	$1.62 \cdot 10^{14}$	0.0121	1.1574	0.01322	129.137	$1.05 \cdot 10^{14}$	0.0533	1.457	0.0007812	155.913	$4.8 \cdot 10^{16}$	20.3
3	2.00	1.1307	115.58	$1.58 \cdot 10^{14}$	0.0121	1.1578	0.01322	129.137	$1.06 \cdot 10^{14}$	0.0536	1.461	0.0007862	155.913	$5.3 \cdot 10^{16}$	21.6
5	1.77	1.1293	115.72	$1.50 \cdot 10^{14}$	0.0120	1.1540	0.01331	129.147	$9.47 \cdot 10^{14}$	0.0052	1.453	0.0007818	155.864	$4.4 \cdot 10^{16}$	18.8
7	1.89	1.1269	115.62	$1.41 \cdot 10^{14}$	0.0116	1.1568	0.01308	129.074	$1.04 \cdot 10^{14}$	0.0525	1.464	0.0007810	155.877	$5.9 \cdot 10^{16}$	21.9
9	1.93	1.1228	115.71	$1.23 \cdot 10^{14}$	0.0113	1.1564	0.01309	129.069	$1.02 \cdot 10^{14}$	0.0527	1.457	0.0007806	155.878	$4.8 \cdot 10^{16}$	20.3
11	1.81	1.1421	115.60	$2.24 \cdot 10^{14}$	0.0135	1.1646	0.01289	129.064	$1.31 \cdot 10^{14}$	0.0571	1.475	0.0007812	155.872	$8.0 \cdot 10^{16}$	25.1
Average		1.131(6)	115.6(6)	$1.6\ (3) \cdot 10^{14}$	0.0027	1.158(4)	0.0131(1)	129.1 (4)	$1.1(1) \cdot 10^{14}$	0.0457	1.4615(8)	0.000782(2)	155.8(2)	$6(1) \cdot 10^{16}$	21.3

Table 4

Details of activation energy (E), maximum temperature (T), distribution width (σ), frequency factors (s), and lifetime (τ) of the TL traps of the peaks 4, 5, and 6 of the CaF_2:La phosphor obtained by the deconvolution method of the glow curves for different doses. Bottom: the average.

Dose (Gy)	FOM (%)	Peak 4: FOK (Continuous)					Peak 5: FOK (Continuous)					Peak 6: FOK (Continuous)				
		E (eV)	σ (eV	T (°C)	s (s^{-1})	τ (year)	E (eV)	σ (eV	T (°C)	s (s^{-1})	τ (year)	E (eV)	σ (eV)	T (°C)	s (s^{-1})	τ (year)
1	2.00	0.914	0.0022302	180.29	$3.0\cdot10^9$	0.1153	1.3916	0.02683	207.421	$1.10\cdot10^{14}$	635.7	1.663	0.0020373	241.16	$5.70\cdot10^{15}$	$1.26\cdot10^7$
3	2.00	0.922	0.0022268	180.29	$3.7\cdot10^9$	0.1030	1.3969	0.02683	207.421	$1.25\cdot10^{14}$	692.6	1.699	0.0020275	241.16	$1.32\cdot10^{16}$	$1.78\cdot10^7$
5	1.77	0.914	0.0022193	180.03	$3.0\cdot10^9$	0.1213	1.4013	0.02640	207.374	$1.40\cdot10^{14}$	738.3	1.719	0.0020341	241.28	$2.09\cdot10^{16}$	$2.12\cdot10^7$
7	1.89	0.927	0.0022292	180.20	$4.3\cdot10^9$	0.1124	1.3995	0.02655	207.408	$1.34\cdot10^{14}$	717.4	1.727	0.0020406	241.63	$2.42\cdot10^{16}$	$1.21\cdot10^7$
9	1.93	0.920	0.0022204	180.27	$3.5\cdot10^9$	0.1567	1.3930	0.02672	207.400	$1.14\cdot10^{14}$	649.0	1.695	0.0020310	241.55	$1.17\cdot10^{16}$	$2.12\cdot10^7$
11	1.81	0.944	0.0022275	180.50	$6.6\cdot10^9$	0.1153	1.4043	0.02659	207.454	$1.50\cdot10^{14}$	777.6	1.728	0.0020353	241.59	$2.52\cdot10^{16}$	$1.26\cdot10^7$
Average		0.92(1)	0.002226(5)	180.3(2)	$4.0(1)\cdot10^9$	0.1186	1.398(5)	0.0267(2)	207.41(3)	$1.3(2)\cdot10^{14}$	701.8	1.70(3)	0.002034(5)	241.4(2)	$1.7(8)\cdot10^{16}$	$1.43\cdot10^7$

Equation (4) has been written using non-geometric parameters, these are the frequency factor (s), the heating rate (β) and the initial concentration of trapped electrons (n_0), in order to establish a relationship between these parameters and the geometric parameters or kinetic parameters, defined as derivation energy (E/E_0), temperature of the maximum (T_{Max}), intensity of the maximum (I_{Max}), amplitude of the contribution (σ) and order of kinetics (b) according to as described by Benavente [18], a maximum condition is used:

$$\left.\frac{dI(T)}{dT}\right|_{T=T_{Max}} = 0 \rightarrow I(T_{Max}) = I_{Max} \tag{7}$$

Then the following mathematical expression can be obtained, where T_{Max}, and I_{Max} are respectively the temperature and intensity of the maximum:

$$\frac{T_{Max}^2}{\beta} = \frac{E}{s\cdot k} exp\left(\frac{E}{k\cdot \mathrm{TMax}}\right) \tag{8}$$

Where k is Boltzmann's constant in (eV/K), E is the activation energy (in eV).

Now (4) can be rewritten in terms of their kinetic parameters, as follow:

$$^{FOK}I_n(T) = I_{Max}\frac{\int f(E)e^{-\frac{E}{kT}}\, exp\left[\frac{-E_0}{kT_{Max}}\left(\frac{T}{T_{Max}}\right)exp\left(\frac{E_0}{kT_{Max}}-\frac{E}{kT}\right)R\left(\frac{E}{KT}\right)\right]dE}{\int f(E)e^{-\frac{E}{kT}}\, exp\left[\frac{-E_0}{kT_{Max}}exp\left(\frac{E_0}{kT_{Max}}-\frac{E}{kT_{Max}}\right)R\left(\frac{E}{kT_{Max}}\right)\right]dE} \tag{9}$$

Glow curves, or TL emission curves, are extremely important for determining kinetic parameters. However, they do not provide information about the recombination centers involved in the TL intensity curve, i.e., the centers responsible for the emission of TL light. Important information about the recombination centers responsible for TL emission can be obtained from the TL emission spectrum, which in practice is a three-dimensional plot whose x, y, and z axes represent temperature (in °C), wavelength (in nm), and TL intensity (in a. u.) respectively. Fig. 8 shows the TL emission spectrum for CaF_2: La phosphor irradiated with a dose of 5 Gy. From the spectrum, we identify just one band extending in the region from 230 to 500 nm, centered at 340 nm (3.65

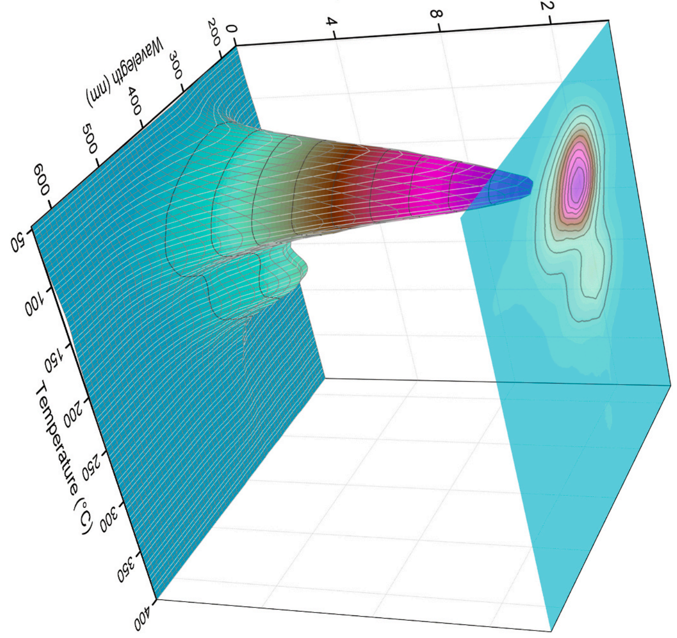

Fig. 8. 3D representation (bottom) and contour plot (top) of the TL spectrum of La-doped CaF_2 phosphor irradiated with a dose of 5 Gy.

eV).

The electron paramagnetic resonance (EPR) spectrum of γ-irradiated CaF_2: La phosphor is shown in Fig. 9. Thermal annealing and microwave (MW) power dependence studies indicate that the observed spectrum has contributions from three defect centers. These centers are labeled in Fig. 9. Fig. 9 also shows the spectrum recorded at low MW power levels (0.1 mW) (see Fig. 9(a)) and high powers (20 mW) (see Fig. 9(b)). At low power levels, center III lines are more intense. On the other hand, center I and II lines are seen more clearly at high powers (20 mW, Fig. 9(b)). Center I is characterized by an axial g-tensor with principal values $g_{\|} = 2.013$ and $g_{\perp} = 2.0053$.

CaF_2 is a member of the alkaline earth halide group and has a crystal structure in the Fm3m space group. In the lattice, the octahedral sites are filled with Ca^{2+} ions, which are bonded to six equivalent F^- ions. The F^- ions, in turn, are surrounded by six Ca^{2+} ions. Both cations and anions are symmetrically arranged such that each Ca^{2+} ion is surrounded by F^- ions and each F^- ion is surrounded by Ca^{2+} ions.

The Ca^{2+} ion has six-fold coordination in the CaF_2 lattice with an ionic radius of 1.0 Å in this six-fold coordination [23]. The La^{3+} ion likely substitutes the Ca^{2+} ion in the lattice because the La^{3+} ion has an ionic radius of 1.03 Å in a six-fold coordination, which is close to that of the Ca^{2+} ion. The charge neutrality requirements will form cation vacancies as the trivalent La^{3+} ion substitutes the divalent Ca^{2+} ion.

The observed EPR line of center I is broad and lacks resolved features (Fig. 9). To understand the intrinsic nature of the EPR spectrum of this center without broadening, the EPR spectrum of center I was simulated using the g-values derived from the observed spectrum, assuming a small linewidth (no broadening from unresolved hyperfine splitting). The simulated spectrum is shown in Fig. 10. This simulated spectrum reveals a clear line shape characteristic of a center with an axially symmetric g-tensor. Further simulations with increasing linewidth were performed, and the final spectrum, with a linewidth of approximately ~9.75 G, matches the experimental spectrum reasonably well. The spectral positions used to determine the g-values of center I are indicated in Fig. 10.

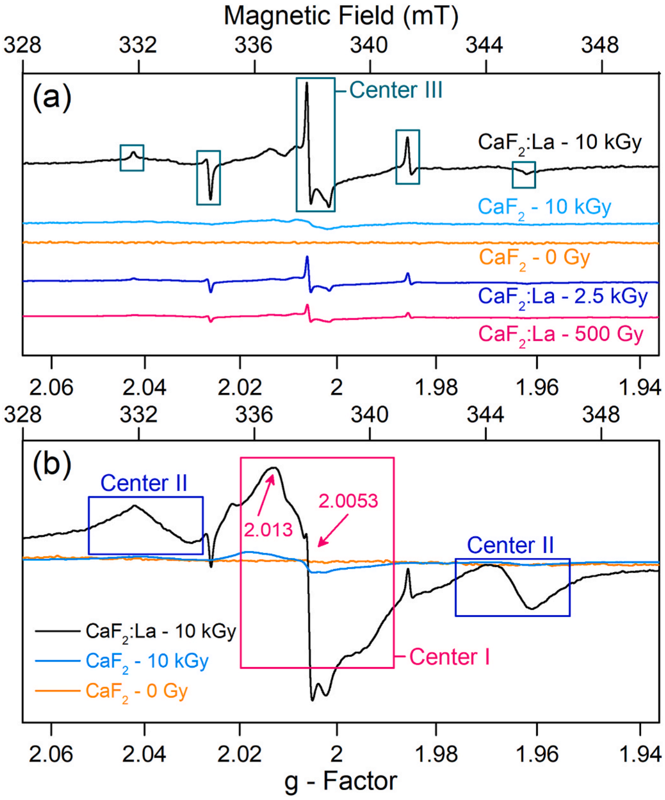

Fig. 9. (a) Room temperature EPR spectrum of γ-irradiated CaF_2: La phosphor (gamma dose: 500 Gy, 2.5 kGy, and 10 kGy). The five green rectangles show the lines from center III. These lines are from an F center. (b) Center I is attributed to an O_2^- ion. Center II is assigned to an F center. The EPR spectrum from the pure CaF_2 sample is also shown. (For interpretation of the references to color in this figure legend, the reader is referred to the Web version of this article.)

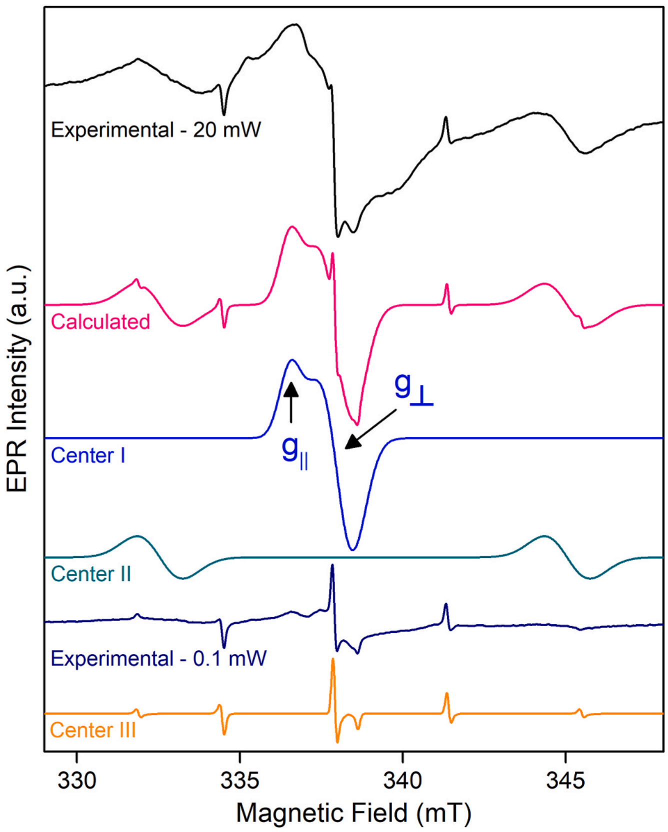

Fig. 10. EPR spectra of La-doped CaF2 phosphor. Experimental with a microwave power of 20 mW (black line), experimental with a microwave power of 0.1 mW (dark blue line), simulated signal (pink line) obtained by summing three spectra (Center I + Center II + Center III). Simulated signal for Center I (blue line), simulated signal for Center II (green line), and simulated signal for Center III (orange line). (For interpretation of the references to color in this figure legend, the reader is referred to the Web version of this article.)

The current study of the CaF_2 powder sample provides limited information on center I, specifically the g-values derived from the spectrum. To identify this center, we need to consider the potential defect centers that gamma irradiation can induce in the CaF_2 system. The most likely defect center in CaF_2 is the F center, which consists of an electron trapped in an F- ion vacancy. The F center typically exhibits an isotropic g-value close to the free-electron value ($g_e = 2.0023$). Study by Bill [24] has shown that the O_2^{2-} ion can be present in the CaF_2 lattice. Upon irradiation, two defect centers can form from the O_2^{2-} ion: the O^- ion and the O_2^- ion. Generally, the O^- ion is characterized by an axial g-tensor, with the perpendicular component being greater than the free-electron value, while the parallel component is close to g_e. An example of this is the O^- ion in MgO [25]. The observed g-values in MgO are $g_{\|} = 2.0016$ and $g_{\perp} = 2.041$. O_2^- ion is also characterized by an axial g-tenor. However, contrary to O^- ion, the perpendicular component is close to the free-spin value while the parallel component is greater than g_e.

Osada et al. [26] observed the oxygen ion (O_2^-) in a study on the binary oxide system Y_2O_3–CaO. EPR investigations revealed that this ion exhibits an axial g-tensor with principal values $g_{\|} = 2.040$ and $g_{\perp} = 2.0030$. This oxygen ion has been identified as the superoxide ion (O_2^-) and is formed by the adsorption of molecular oxygen by the binary oxide system. The O_2^- ion, which exhibits significant g-anisotropy, has also been detected in various zeolites and metal oxides [27–29]. In these systems, the $g_{||}$ value is highly dependent on the host lattice and ranges between 2.0150 and 2.080.

Comparing the observed *g*-values in the present system with that of the above three centers (F center, O^- ion, and O_2^- ion), center I is tentatively assigned to an O_2^- ion. It may be mentioned that the O_2^- ion has been previously observed in CaF_2 single crystal by Bill [24]. The ion displayed a rhombic *g*-tensor with principal values $g_1 = 2.0038$, $g_2 = 2.0092$, and $g_3 = 2.0178$ at 292 K. Bill [24] proposed a model of the O_2^- ion in the CaF_2 lattice, and the model is shown in Fig. 11. As per this model, the O_2^- ion in CaF_2 originates from an O_2^{2-} molecule located in the space left by two missing mutually neighboring F ions. A neighboring cation vacancy accompanies the O_2^- ion. This model is derived from the results of Raman and EPR studies carried out by Bill [24]. The neighboring cation vacancy provides stability to the ion.

A pulsed thermal annealing method was used to study the stability of center I. The method involves heating the sample to a particular temperature and then the sample is kept at this temperature for 3 min. Later the sample is cooled to room temperature for EPR experiments. The thermal annealing behavior of center I is shown in Fig. 12. It is observed that the center becomes unstable at about 155 °C and decays in the temperature range 155 and 320 °C. Based on this behavior, it is inferred that center I is associated with the TL peak at 205 °C in the CaF_2: La phosphor.

Gamma irradiation can induce the formation of F centers, which are electrons trapped at an anion vacancy, in alkaline-earth halide systems such as CaF_2. In the first observation of an F center in an alkali halide system, a relatively large linewidth of about 100 G was observed, as reported by Hutchinson [30]. However, in MgO, the inherent linewidth of the center was observed to be quite small, about 1 G [31]. The observed linewidth is determined by the delocalization of the unpaired electron and its subsequent interaction with neighboring ions. The relative abundance of isotopes and their respective magnetic moments of neighboring ions also play a role in determining the linewidth. In alkali halides, there is considerable delocalization of the unpaired electron, resulting in interaction with immediate neighbors and alkali and halide ions in successive neighboring shells. For example, large linewidths of 20 G and 58 G were observed in KCl and LiCl respectively [32].

During irradiation, an anion vacancy captures an electron forming an F center, which displays positive and negative *g*-shifts. The observed *g*-value of F centers is close to the free-electron value of 2.0023. Center II in CaF_2: La has a *g*-value of 2.0005 and a linewidth of 14 G. Based on the known features of the F center, center II is tentatively identified as the F center. Anion vacancies are likely to be present in CaF_2 and these vacancies can trap electrons to form F centers. Center II displays a two-line spectrum and the two lines can be explained by the unpaired spin's interaction with a nearby fluorine ion which has a nuclear spin of ½. The hyperfine splitting is estimated to be 103 G. The large linewidth of the individual lines suggests the presence of additional hyperfine interaction. This unresolved hyperfine structure may arise from the nuclear spins nearby interacting with the center. The isotope of fluorine that can potentially interact with the unpaired spin and cause the broad line is ^{19}F, which has 100 % abundance and a magnetic moment of 2.6 [33].

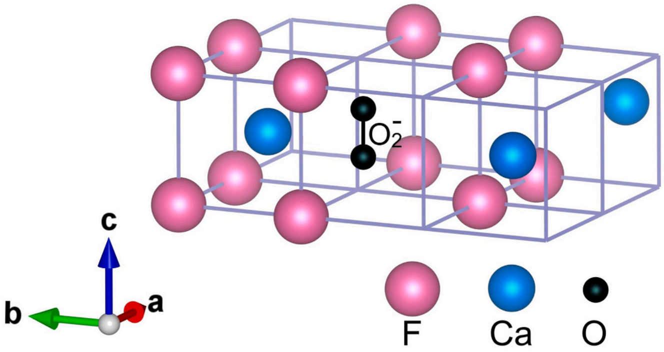

Fig. 11. Model of O_2^- ion in the CaF_2 lattice as derived from EPR and Raman results [24].

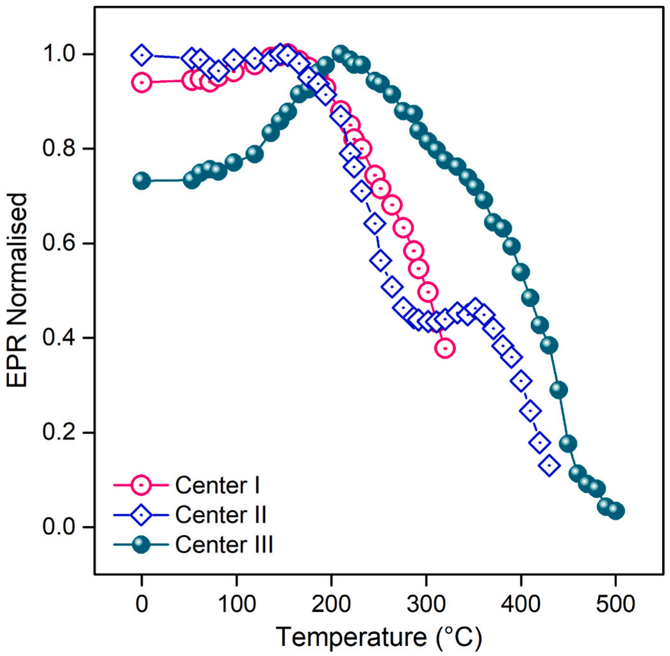

Fig. 12. Thermal annealing behavior of center I (O_2^- ion), center II (F center), and center III (F center) in CaF_2: La phosphor.

Well-resolved hyperfine splitting has also been reported in various systems. For example, in a study on SrO single crystals, Culvahouse et al. [34] report a hyperfine interaction of the F^+ electron (one electron in an O^{2-} vacancy) with the nearest neighbor (nn) Sr^{87} nuclei. The hyperfine splitting is resolved and the isotropic part (the dominant part) of the hyperfine interaction is observed to be A = 14.7 G and the dipolar part is small (B ~ 1.6 G). Similarly, in BaO [35], the F^+ center exhibits resolved hyperfine splitting as the unpaired electron interacts with the nearby Ba nucleus. There are two magnetic isotopes Ba^{135} and Ba^{137}. Resolved hyperfine splitting is seen due to both isotopes (the isotropic part of the splitting is 68.2 G and 76.4 G for Ba^{135} and Ba^{137} respectively). Additionally, resolved hyperfine splitting is observed in α-Al_2O_3 [36] where a broad spectrum with 13 resolved components is reported for the F^+ center.

Fig. 12 illustrates the thermal annealing characteristics of center II. The ESR lines linked with center II exhibit two phases of intensity reduction. The initial phase spans from roughly 156 °C–290 °C and is characterized by the recombination of charges that were released from other defect centers with center II. It is plausible that the holes discharged from center I are combined with center II, implying that center II could function as a recombination center associated with the TL peak at 205 °C. The second phase of intensity reduction for center II occurs from 350 °C to 430 °C and corresponds to the actual decay of center II.

The EPR lines labeled as center III in Fig. 9 arise from a single species and are due to a center characterized by an axially symmetric *g*-tensor with principal values $g_{||} = 2.0016$ and $g_{\perp} = 2.0057$. The center exhibits hyperfine splitting due to the interaction of the unpaired spin with two equivalent spin ½ nuclei resulting in the spectrum shown in Fig. 9. The hyperfine tensor is also axially symmetric with principal values $A_{||} = 68$ Gauss and $A_{\perp} = 35$ Gauss.

In general, F centers (halide anion vacancy with one electron) are characterized by an isotropic *g*-value, and center III in the present system exhibits an axially symmetric *g*-tensor. Systems like Yttria stabilized

Zirconia (YSZ) [37], as well as CaZrO3: Tb [38], display a center that shows axially symmetric *g*-values. For example, in YSZ, the principal *g*-values are $g_{||} = 1.996$ and $g_{\perp} = 1.972$. It is observed that the *g*-values are smaller than the free-spin value. The center in these two systems was identified as the F^+ center (oxygen vacancy with one electron). Costantini et al. [37], in their study on YSZ interpreted the axial nature of the *g*-values by considering the presence of a symmetry-breaking defect at an anion site close to the F^+ center. They considered the symmetry braking defect to be the neutral F center (oxygen vacancy with two electrons) which has a high probability of forming in YSZ lattice due to the presence of a large density of oxygen vacancies in the YSZ lattice. Center III in the present system is also tentatively attributed to an F center (an electron trapped in a halide vacancy) and this center needs to be close to an entity (like the F center in YSZ) that gives rise to the observed features. It is to be noted that X-irradiated sodium β-alumina [39] also displays an axial *g*-tensor with positive *g*-shifts as observed for center III. It has not been possible to identify the symmetry-breaking defect in the present study.

The thermal annealing behavior of center III is displayed in Fig. 12. The EPR lines associated with the center exhibit two phases of intensity changes. In the initial phase spanning from 80 °C to 210 °C, the intensity increases and indicates the increase in the concentration of center III. A possible explanation for this increase is as follows. After gamma irradiation, there are still precursors of center III present in the lattice. Assuming these precursors to have a higher cross section for the capture of charges, the charges released from unknown defect centers during thermal annealing are trapped by the precursors to form center III. This will appear as an increase in the intensity of center III EPR lines. In the second phase ranging from 210 °C to 500 °C, the center exhibits instability at about 210 °C and undergoes decay within this temperature range.

In the EPR spectrum presented in Fig. 9, it is observed that centers I and II increase in intensity with MW power while center III intensity appears to be almost the same. It thus appears that center III has a longer relaxation time as compared to the other two centers. Similar behavior is observed for the defect centers observed in irradiated Quartz. In quartz, three defect centers are observable at room temperature: the E', the Ge, and the peroxy centers. The E' center saturates at very low MW powers (~0.1 mW) while the other two centers saturate at high MW powers. Saturation at very low powers is a characteristic feature of the E' center. Center II and Center III are attributed to an F^+ center. Both exhibit hyperfine interaction with nearby nuclei and apart from this there are no apparent differences and it is difficult to understand the different relaxation times.

EPR spectra of centers I, II, and III were simulated and the simulated spectra are shown in Fig. 10. The principal *g* and *A* values derived from the experimental spectrum were used in this simulation. Apart from the individual spectra corresponding to the three centers, the overall spectrum was obtained by combining all three spectra and this spectrum is also displayed in Fig. 10. It is seen that the simulated spectrum reasonably matches the experimental spectrum.

4. Conclusions

In this work, we study for the first time the TL properties in combination with the EPR properties of La-doped CaF_2 phosphor. The concentration of the dopant does not interfere with the crystal structure of the material, as confirmed by XRD results. The CaF_2 phosphor doped with 0.3 mol% La presented a higher sensitivity in its TL light emission. The structure of the glow curve of the La-doped CaF_2 phosphor presents two peaks centered at 130 and 205 °C and an emission band between 230 and 500 nm centered at 340 nm. Both peaks present a linear behavior in the dose range from 1 to 9 Gy. From the deconvolution analysis of the TL glow curves for different doses of gamma radiation, it was shown that it is formed by the superposition of six peaks that obey first-order kinetics. Also, trap depths, TL peak positions, and frequency factors were estimated for all peaks. These TL results for CaF_2: La phosphor confirm good future possibilities in the field of TL dosimetry. Three defect centers have been identified in the irradiated CaF_2: La phosphor. These centers are tentatively assigned to an O_2^- ion, and two F centers. O_2^- ion correlates with the 205 °C TL peak while the F center (center II) appears to act as a recombination center for the 205 °C TL peak. No specific TL role could be assigned to Center III.

CRediT authorship contribution statement

Jessica Mosqueira-Yauri: Visualization, Investigation, Formal analysis, Data curation, Conceptualization. **T.K. Gundu Rao:** Writing – original draft, Validation, Supervision, Investigation, Data curation, Writing – review & editing. **Joel A. Rivera-García:** Methodology, Investigation. **Klinton V.T. Huahuasoncco:** Software, Investigation, Formal analysis. **Jorge S. Ayala-Arenas:** Validation, Supervision, Investigation, Formal analysis. **J.F. Benavente:** Validation, Software, Methodology, Investigation, Formal analysis. **L.M. Rondán-Flores:** Investigation, Formal analysis. **José F.D. Chubaci:** Investigation. **Nilo F. Cano:** Writing – original draft, Visualization, Validation, Supervision, Project administration, Investigation, Conceptualization, Writing – review & editing.

Declaration of competing interest

The authors declare that they have no known competing financial interests or personal relationships that could have appeared to influence the work reported in this paper.

Acknowledgements

The authors would like to express thanks to Ms. E. Somessari from the Institute for Energy and Nuclear Researches (IPEN/CNEN-SP), Brazil, for kindly carrying out the γ-irradiation of the samples, and the “Central de Analises Multiusuario” laboratory of IPEN/CNEN-SP for the SEM measurements. This work was supported by PROCIENCIA-CONCYTEC, Peru, in the framework of the call E041-2023-01 (Process number PE501082822-2023 -PROCIENCIA).

References

[1] J. Azorin, Preparation methods of thermoluminescent materials for dosimetric applications: an overview, Appl. Radiat. Isot. 83 (2014) 187–191, https://doi.org/10.1016/j.apradiso.2013.04.031.

[2] A.S. Mukasyan, P. Epstein, P. Dinka, Solution combustion synthesis of nanomaterials, Proc. Combust. Inst. 31 (2007) 1789–1795, https://doi.org/10.1016/j.proci.2006.07.052.

[3] M. Sohrabi, F. Abbasisiar, M. Jafarizadeh, Dosimetric characteristics of natural calcium fluoride of Iran, Radiat. Protect. Dosim. 84 (1999) 277–280, https://doi.org/10.1093/oxfordjournals.rpd.a032737.

[4] M. Topaksu, A.N. Yazici, The thermoluminescence properties of natural CaF_2 after β-irradiation, Nucl. Instrum. Methods B 264 (2007) 293–301, https://doi.org/10.1016/j.nimb.2007.09.018.

[5] V.K. Asfora, V.S.M. Barros, R.J.G. Silva, D.A.A. Vasconcelos, B.S. Nobre, M. E. Yamato, H.J. Khoury, R.A. Oliveira, W.M. Azevedo, Optically stimulated luminescence of CaF_2:Tm, Radiat. Meas. 85 (2016) 73–77, https://doi.org/10.1016/j.radmeas.2015.12.012.

[6] G. Aldica, M. Secu, Investigations of the non-isothermal crystallization of CaF_2 nanoparticles in Sm-doped oxy-fluoride glasses, J. Non-Cryst. Solids 356 (2010) 1631–1636, https://doi.org/10.1016/j.jnoncrysol.2010.06.017.

[7] M. Topaksu, V. Correcher, J. Garcia-Guinea, Luminescence emission of natural fluorite and synthetic CaF_2:Mn (TLD-400), Radiat. Phys. Chem. 119 (2016) 151–156, https://doi.org/10.1016/j.radphyschem.2015.10.002.

[8] G. Leniec, S.M. Kaczmarek, G. Boulon, EPR and optical properties of CaF_2:Yb single crystals, Proc. SPIE 5958, Lasers Appl. (2005) 595825, https://doi.org/10.1117/12.622501.

[9] N. Salah, N.D. Alharbi, S.S. Habib, S.P. Lochab, Luminescence properties of CaF_2 nanostructure activated by different elements, J. Nanomater. 16 (2015) 1–7, https://doi.org/10.1155/2015/136402.

[10] D.A.A. Vasconcelos, V.S.M. Barros, H.J. Khoury, W.M. Azevedo, V.K. Asfora, P. L. Guzzo, Synthesis and thermoluminescent response of CaF_2 doped with Tm^{3+}, Radiat. Meas. 71 (2014) 51–54, https://doi.org/10.1016/j.radmeas.2014.05.027.

[11] E. Aşlar, E. Şahiner, A thermoluminescence study of CaF_2:Dy under different types of irradiation sources towards environmental dosimetric applications, J. Lumin. 249 (2022) 119012, https://doi.org/10.1016/j.jlumin.2022.119012.

[12] R. Rodríguez, V. Correcher, J.M. Gómez-Ros, J.L. Plaza, Preliminary study on the thermoluminescence properties of CaF_2 and Tm_2O_3 pellets, Nucl. Instrum. Methods A 959 (2020) 163561, https://doi.org/10.1016/j.nima.2020.163561.

[13] X. Xie, B. Mei, J. Song, W. Li, L. Su, Fabrication and spectral properties of Nd, La: CaF_2 transparent ceramics, Opt. Mater. 76 (2018) 111–116, https://doi.org/10.1016/j.optmat.2017.12.033.

[14] D.A.A. de Vasconcelos, V.S.M. Barros, H.J. Khoury, V.K. Asfora, R.A.P. Oliveira, Thermoluminescent dosimetric properties of CaF_2:Tm produced by combustion synthesis, Radiat. Phys. Chem. 121 (2016) 75–80, https://doi.org/10.1016/j.radphyschem.2015.12.017.

[15] J.A. Rivera-García, J. Mosqueira-Yauri, T.K. Gundu Rao, E.A. Canaza-Mamani, G. G. Fiorini, J.F. Benavente, C.D. Gonzales-Lorenzo, J.F.D. Chubaci, S. Watanabe, J. S. Ayala-Arenas, N.F. Cano, Synthesis and thermoluminescence of Ce-doped CaF_2 phosphor: study of defect centers responsible for the TL emission by EPR analysis, J. Lumin. 261 (2023) 119906, https://doi.org/10.1016/j.jlumin.2023.119906.

[16] P.R. González, D. Mendoza-Anaya, L. Mendoza, L. Escobar-Alarcón, Luminescence and dosimetric properties of CaF_2:Ce,Dy phosphor, J. Lumin. 195 (2018) 321–325, https://doi.org/10.1016/j.jlumin.2017.11.050.

[17] S.W.S. McKeever, Thermoluminescence of Solids, Cambridge University Press, London, 1985.

[18] J.F. Benavente, J.M. Gómez-Ros, A.M. Romero, Thermoluminescence glow curve deconvolution for discrete and continuous trap distributions, Appl. Radiat. Isot. 153 (2019) 108843, https://doi.org/10.1016/j.apradiso.2019.108843. Article.

[19] H.G. Balian, N.W. Eddy, Figure of merit (FOM), an improved criterion over the normalised chi-squared test for assessing goodness-of-fit of gamma ray spectra peaks, Nucl. Instrum. Methods 145 (1977) 389–395, https://doi.org/10.1016/0029-554X(77)90437-2.

[20] K.V.R. Murthy, Thermoluminescence and its applications: a review, Defect Diffusion Forum 347 (2013) 35–73. https://doi.org/10.4028/www.scientific.net/ddf.347.35.

[21] J.A. Nieto, Thermoluminescence dosimetry (TLD) and its application in medical physics, AIP Conf. Proc. 724 (2004) 20–27, https://doi.org/10.1063/1.1811814.

[22] T. Rivera, Thermoluminescence in medical dosimetry, Appl. Radiat. Isot. 71 (2012) 30–34, https://doi.org/10.1016/j.apradiso.2012.04.018.

[23] R.D. Shannon, Revised effective ionic radii and systematic studies of interatomic distances in halides and chalcogenides, Acta Crystallogr. A32 (1976) 751–767, https://doi.org/10.1107/S0567739476001551.

[24] H. Bill, Motional effects in the EPR spectrum of an O_2^- molecule ion in natural CaF_2 crystals, Solid State Commun. 15 (1974) 911–915, https://doi.org/10.1016/0038-1098(74)90692-9.

[25] W.B. Williamson, J.H. Lunsford, C. Naccache, The EPR spectrum of O^- on magnesium oxide, Chem. Phys. Lett. 9 (1971) 33–34, https://doi.org/10.1016/0009-2614(71)80174-4.

[26] Y. Osada, S. Koike, T. Fukushima, S. Ogasawara, T. Shikada, T. Ikariya, Oxidative coupling of methane over Y_2O_3 single bond CaO catalysts, Appl. Catal. 59 (1990) 59–74, https://doi.org/10.1016/S0166-9834(00)82187-9.

[27] D.D. Eley, M.A. Zammitt, Spin centers and catalysis on γ-alumina, J. Catal. 21 (1971) 366–376, https://doi.org/10.1016/0021-9517(71)90156-4.

[28] K.M. Wong, J.H. Lunsford, An electron paramagnetic resonance study of Y-type zeolites. III O_2^- on AIHY, SCY, and LaY zeolites, Phys. Chem. 74 (1971) 1165–1168.

[29] J.H. Lunsford, ESR of adsorbed oxygen species, Catal. Rev. 8 (1974) 135–157, https://doi.org/10.1080/01614947408071859.

[30] C.A. Hutchison, Paramagnetic resonance absorption in crystals colored by irradiation, Phys. Rev. 75 (1949) 1769–1770, https://doi.org/10.1103/PhysRev.75.1769.2.

[31] J.E. Wertz, P. Auzins, R.A. Weeks, R.H. Silsbee, Centers in magnesium oxide; confirmation of the spin of magnesium-25, Phys. Rev. 107 (1957) 1535–1537, https://doi.org/10.1103/PhysRev.107.1535.

[32] W.C. Holton, H. Blum, Paramagnetic resonance of F centers in alkali halide, Phys. Rev. 125 (1962) 89–103, https://doi.org/10.1103/PhysRev.125.89.

[33] R.C. Weast (Ed.), Handbook of Chemistry and Physics, CRC, Cleveland, 1971.

[34] J.W. Culvahouse, L.V. Holroyd, J. Kolopus, F centers in SrO and the quadrupole moment of ^{87}Sr, Phys. Rev. 140 (A) (1965) 1181, https://doi.org/10.1103/PhysRev.140.A1181.

[35] K.E. Mann, L.V. Holroyd, D.L. Cowan, F-Centers in BaO, Phys. Stat. Solidi 33 (1969) 391, https://doi.org/10.1002/pssb.19690330137.

[36] S.Y. La, R.H. Bartram, R.T. Cox, The F^+ center in reactor-irradiated aluminum oxide, J. Phys. Chem. Solid. 34 (1973) 1079–1086, https://doi.org/10.1016/S0022-3697(73)80016-2.

[37] J.M. Costantini, F. Beuneu, D. Gourier, C. Trautmann, G. Calas, M. Toulemonde, Colour centre production in yttria-stabilized zirconia by swift charged particle irradiations, J. Phys. Condens. Matter 16 (2004) 3957, https://doi.org/10.1088/0953-8984/16/23/014.

[38] Vijay Singh, S. Watanabe, T.K. Gundu Rao, Katharina Al-Shamery, M. Haase, Y. D. Jho, Synthesis, characterisation, luminescence and defect centres in solution combustion synthesised $CaZrO_3$:Tb^{3+} phosphor, J. Lumin. 132 (2012) 2036–2042, https://doi.org/10.1016/j.jlumin.2012.03.027.

[39] K. O'Donnell, R.C. Barklie, B. Henderson, EPR and optical absorption studies of radiation-produced defects in sodium beta-alumina, J. Phys. C Solid State Phys. 11 (1978) 3871, https://doi.org/10.1088/0022-3719/11/18/022.